Microseismic imaging of a geothermal reservoir stimulation

B. C. Dyer, Semore Seismic, Cornwall, U. K.
U. Schanz, F. Ladner, and M. O. Häring, Geothermal Explorers LTD, Pratteln, Switzerland
T. Spillman, NAGRA, Wettingen, Switzerland

Exploitation of geothermal heat energy from rocks at depths of several km has been the goal of various projects since the mid-1970s. To exploit the energy in these deep rocks poses technical challenges in drilling, well completion, creation of the heat exchange reservoir at depth, and control of seismicity. In spite of the difficulties, what are now known as enhanced/engineered geothermal systems (EGS) offer almost limitless clean energy, so it is not surprising that this technology continues to attract investors. However, commercial energy production from the greatest potential resource, hot rock at depths >5 km or temperatures >200° C, remains elusive.

The basic principle in exploiting the heat energy in rocks at depth is to circulate water through the rock to extract the heat. Typically the targeted rocks are not porous and the flow paths are through natural fractures. To achieve economic flow rates, the natural fractures commonly require stimulation to reduce the flow impedance. Stimulation can generate thousands of microseismic events and, critically, a few small earthquakes that may be felt at the surface. The microseismic and hydraulic data derived from the stimulation enable evaluation of the potential for developing a fractured reservoir. In addition, the earthquake magnitudes may determine if development is even possible (i.e., if the magnitudes exceed local limits or cause public concern).

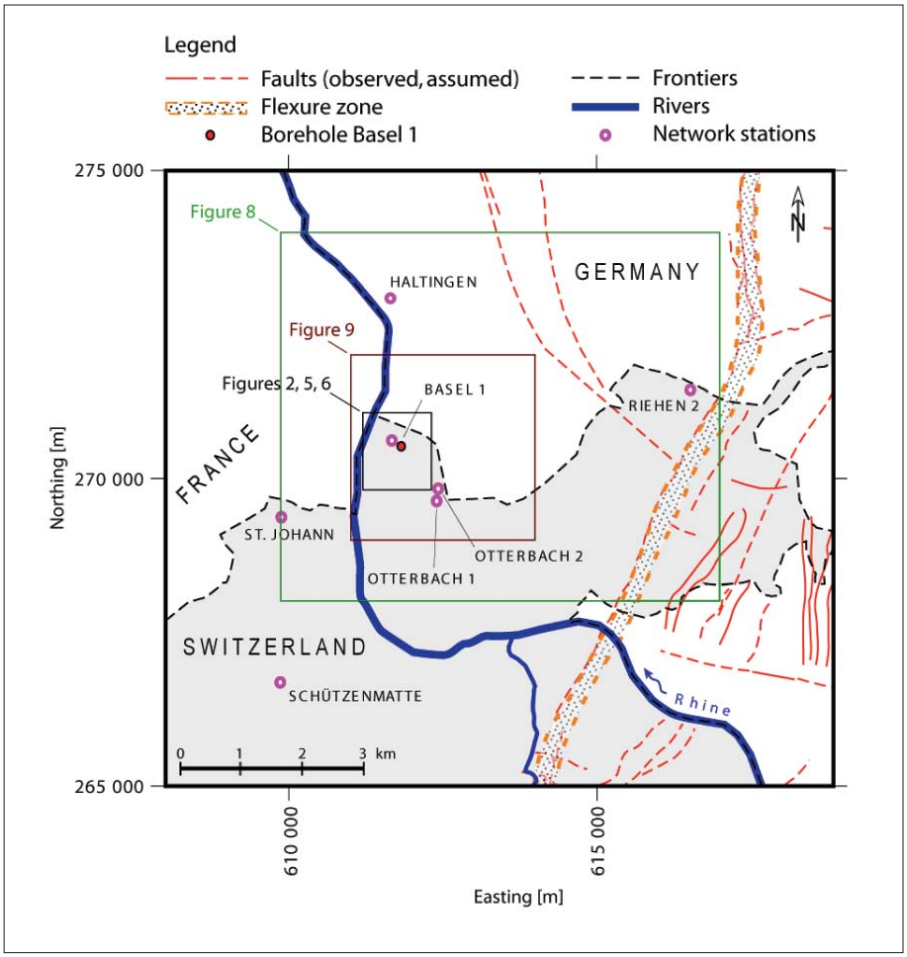

Figure 1. *Tectonic map of the Upper Rhine Graben. Borehole Basel 1 is shown by a red dot and the microseismic monitoring network stations as pink circles. The frames indicate the boundaries in subsequent figures. (After Gürler et al., 1987).*

The subject of this paper is an EGS project in Basel, Switzerland to create a cogeneration pilot plant producing both electrical and thermal energy. As the project is within the city, the potential for generating earthquakes was a critical consideration and installation/operation of a sensitive, highly reliable seismic monitoring system was a priority.

In order to locate the microseismic events, an accurate velocity model was required. This article describes how a deep seismic sensor in the stimulation well made it possible to derive the velocity model directly from the microseismic data. Real-time monitoring of the microseismic event distribution enabled observation of the growth of the stimulated region and the evalutation of the reservoir properties. We also show how potential fractures, not stimulated but of interest for developing the reservoir, may be imaged by migration of the microseismic data.

Geologic and tectonic framework

The Basel project is in the Upper Rhine Graben (Figure 1) that forms part the European Cenozoic rift system. Extension in the Upper Rhine Graben was controlled by pre-existing structures in the basement and accommodated by the formation of normal faults and flexures. Several NNE–SSW and NW–SE fault systems of various ages are known in the eastern part of the area.

The azimuth of the maximum horizontal principal stress (SHmax) has been deduced from log analysis in the granite section of Basel 1. The direction of SHmax was determined from borehole breakouts as N143±14°E and from drilling-induced tensile fractures as N151±13°N (Valley and Evans, 2006). The fracture strike directions, also measured from logs, were predominantly in the range 140–170°. These measurements agree with previous estimates (150° and 145°) of the direction of SHmax (Plenefisch und Bonjer, 1997; Evans and Roth, 1997). The maximum horizontal stress direction is a result of the alpine compression, the dominant mechanism

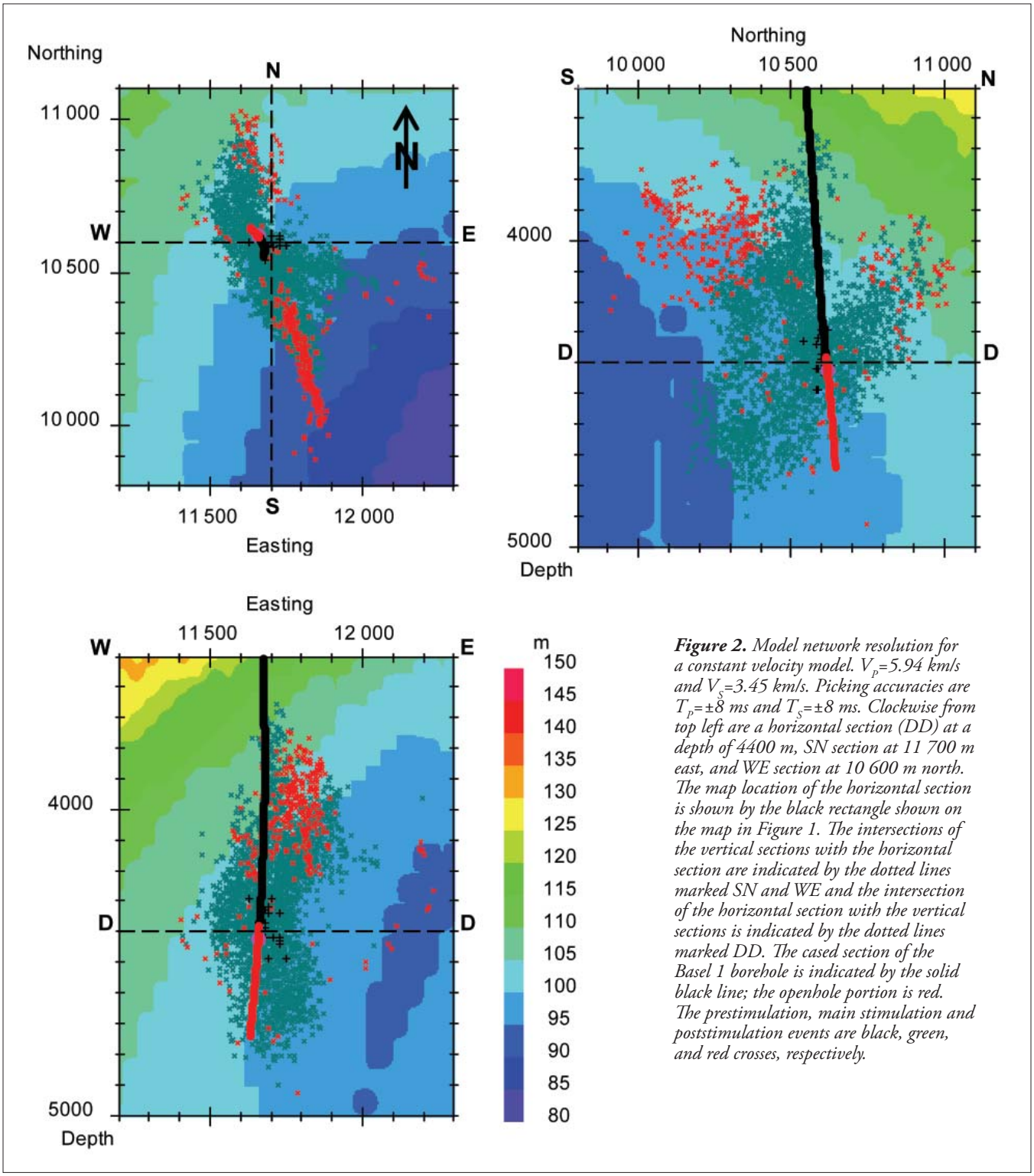

Figure 2. *Model network resolution for a constant velocity model. V_P=5.94 km/s and V_S=3.45 km/s. Picking accuracies are T_P=±8 ms and T_S=±8 ms. Clockwise from top left are a horizontal section (DD) at a depth of 4400 m, SN section at 11 700 m east, and WE section at 10 600 m north. The map location of the horizontal section is shown by the black rectangle shown on the map in Figure 1. The intersections of the vertical sections with the horizontal section are indicated by the dotted lines marked SN and WE and the intersection of the horizontal section with the vertical sections is indicated by the dotted lines marked DD. The cased section of the Basel 1 borehole is indicated by the solid black line; the openhole portion is red. The prestimulation, main stimulation and poststimulation events are black, green, and red crosses, respectively.*

for natural seismic activity in the area, and not the extension of the Rhine graben, a failed rift system that predates the forces acting at present.

The depths of the major lithological units were interpreted from cuttings and well logs after drilling the Basel 1 borehole. The granitic basement was found at ~2257 m bOD (below Ordnance Datum), overlain by the Carboniferous/Permian from ~1396 m bOD and the Mesozoic from ~147 m bOD with Tertiary sediments and a thin alluvial layer above. The local ground surface is at 251 m aOD (above Ordnance Datum).

Monitoring system

The microseismic monitoring network consisted of six permanent, three-component downhole geophones. Four were installed at moderate depths in wells Otterbach 1, Haltingen, St. Johann, and Schützenmatte (Figure 1) between 325 and 550 m below the surface. The geophone in Riehen 2 was at 1178 m, and the deepest geophone in Otterbach 2 is in the granite at 2738 m below the surface. A special 200°C, 100 MPa geophone tool was built and temporarily installed in Basel 1 to calibrate the seismic velocity model. The tool was intended to rest on the bottom of the well but stopped

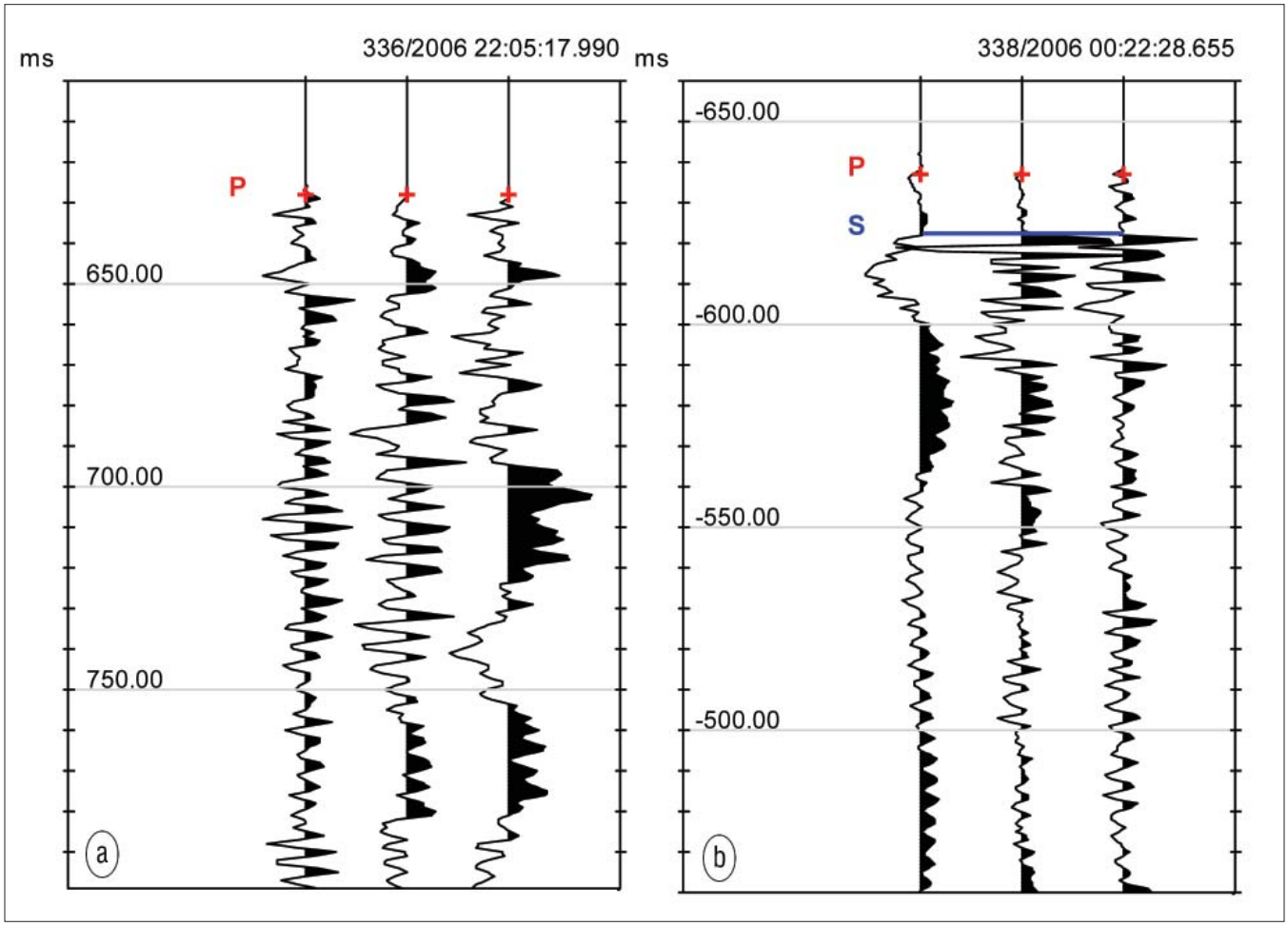

Figure 3. *Two events recorded by the geophone in Basel 1. The traces are displayed in the order vertical, horizontal 1 and horizontal 2. The group on the left is from the first event located and does not have a distinct S-wave arrival. The group on the right, recorded around 26 hours later, has distinct P and S arrivals. The P-to-S time difference corresponds to an event offset from the sensor of around 115 m.*

at 4422 m bOD where the borehole had become impassable, but not hydraulically blocked, during prestimulation hydraulic tests.

In view of the known natural seismicity and the potential seismic risks, a major goal was an understanding of the natural microseismicity prior to any hydraulic tests. Installation of the seismic monitor system commenced three months prior to drilling the first EGS well (Basel 1) and was fully operational six months prior to the first hydraulic injection so that the drilling of the second half of the well in the hot, fractured granite could be fully monitored. Continuous operation of the monitoring system during the drilling and subsequent stimulation of the well was critical to monitoring and provided an immediate response to significant perceptible earthquakes or ground shaking. To achieve this, data were continuously transferred via a virtual private network (VPN) link to the central server. The acquisition system and the data were continuously backed up to computer disk and optical storage media.

The injection rate and hydraulic pressure were monitored at the wellhead and hydraulic pressure was also monitored at depth. Unfortunately, after the prestimulation test, the borehole was impassable at 4422 m bOD, and downhole logging could not be conducted below this depth.

Prior to the stimulation experiments, the network resolution was tested by analyzing the location errors over a synthetic hypocenter grid with 50-m spacing. P- and S-wave traveltimes from each grid point to the receivers were compared with traveltimes from trial locations. By limiting the maximum traveltime differences between the grid point and trial location, for each receiver, to the picking accuracy of ±8 ms, an error surface around each grid point was obtained. The resolution was defined as the maximum distance between the grid point and the error surface. The method available at the time required constant V_P and V_S velocities rather than the two-layer model used for the actual locations, and so the error values should be treated as estimates. However, from this analysis of the network resolution, it was found that the monitoring stations St. Johann and Otterbach 1 had relatively little influence on the resolution and did not need to be routinely processed.

The resolution of a network of Haltingen, Schützenmatte, Riehen, and Otterbach 2 is shown in Figure 2 for a horizontal slice at the reservoir depth and two vertical sections. These estimated errors are consistent with the traveltime misfits of the real locations and the apparent resolution of the locations that can be assessed from the dimensions of the seismically mapped features in the hypocenter distribution. It should be noted that the resolution shown is the relative resolution between events due to the traveltime picking accuracy. The

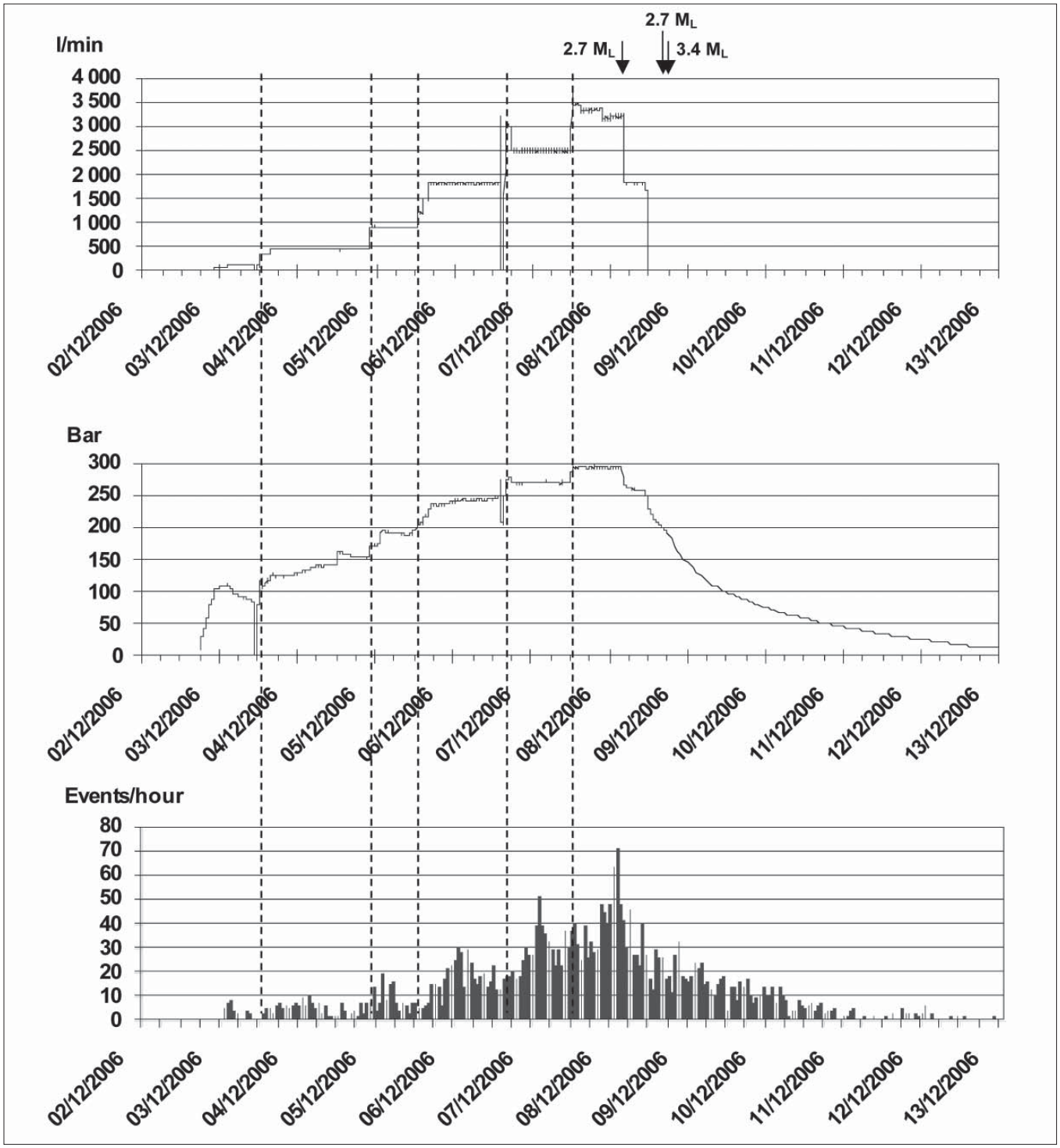

Figure 4. *Basel 1 main stimulation hydraulic and seismic data: (top to bottom) the injection rate, surface injection pressure, and the located seismic event rate. The anomalous hydraulic values on 3/12 and 6/12 relate to periods in which the injection pumps were exchanged. The three largest events that occurred during the stimulation and shut-in phases are indicated.*

absolute resolution depends on the accuracy of the velocity model as well.

Seismic response procedure

Prior to the stimulation, a response procedure was devised that specified actions for a range of scenarios. This system was based on the "traffic light" scheme of Bommer et al. (2006). Three independent criteria were considered: responses from the public, local magnitude (M_L), and peak ground velocity (PGV). The M_L and PGV levels were derived from simulations of surface ground motion based on real data from the Soultz-sous-Forêts EGS project (Baria et. al., 2006) and the geologic situation (microzonation) in Basel (Rutishauser, 2006).

It was not possible to quantify the public response in advance. However, the interpretation of the public response was the overriding consideration.

The local earthquake magnitude (M_L) and ground velocity were provided by the Swiss Seismological Service (SED). This independent monitoring also ensured consistency with

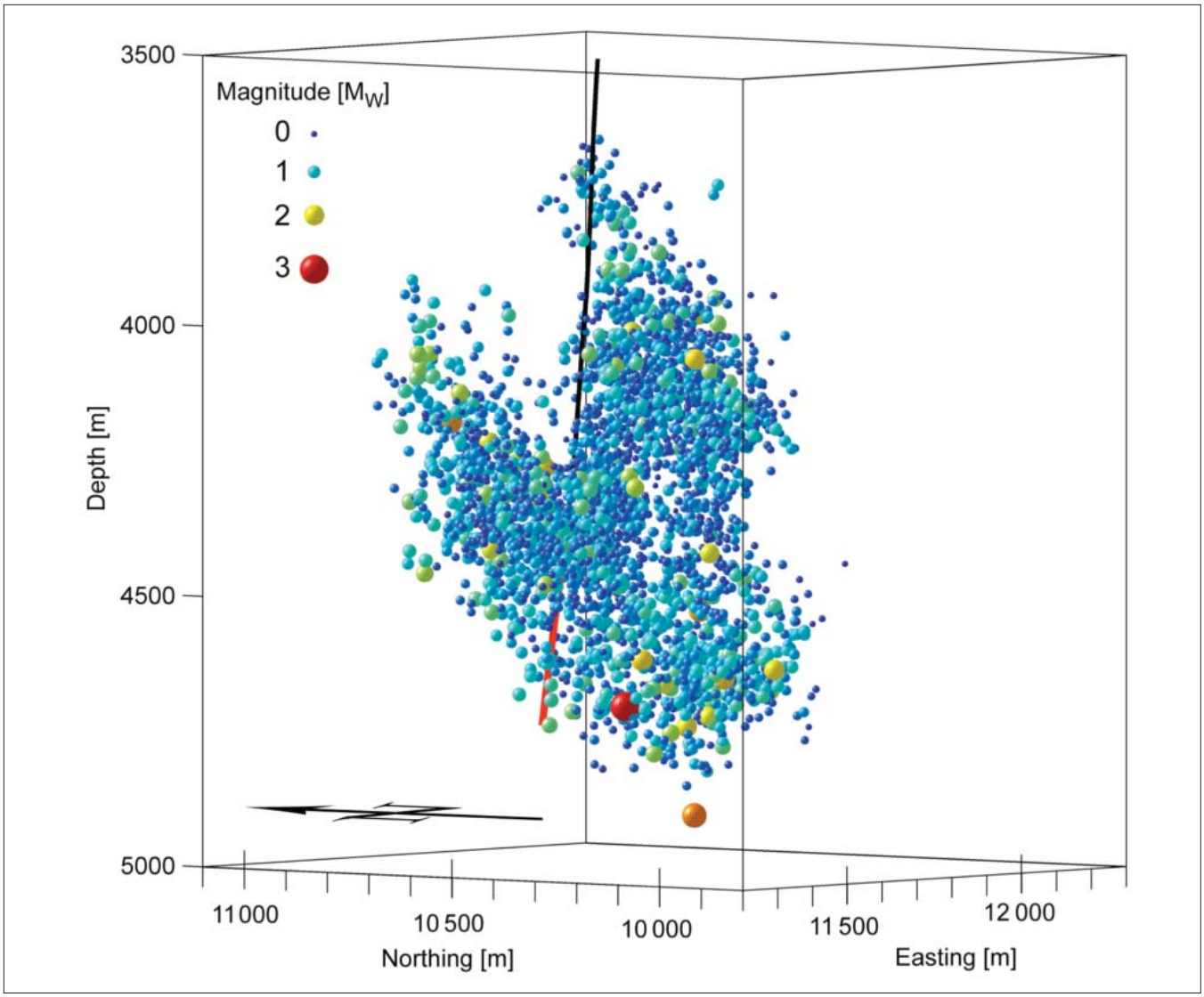

Figure 5. *3D view of the microseismic events detected during the main stimulation with the event symbols colored and scaled according to the moment magnitudes.*

the magnitudes of regional earthquakes.

The permanent microseismic network provided alternate measures of the moment magnitude (M_W) that could be loosely related to the SED-measured M_L. The real-time processing software continuously monitored these levels and incorporated internal audible alarms and visual updates to alert the operators. This system was staffed 24 hours a day during the stimulation by at least one geophysicist and an operator.

Velocity model

As all sensors were in the sediments or granite, a velocity model with two horizontal layers (sediments and crystalline) was considered appropriate. Initially, average P- and S-velocities in each layer were obtained from sonic velocity measurements. In principle, the average velocities in the sediments and granite could have been refined by firing check shots in the well over the reservoir interval. However, due to the proximity of domestic properties and radio interference, it would have been necessary to use radio-frequency-safe detonators. Such detonators were available but had a 150°C temperature limit that would have required prior cooling of the well. This was possible, but two alternative methods were tested.

In the first, a drilling jar was fired just below the top of the granite to measure the sediment velocities directly and as a transmission test from an interim depth prior to the planned terminal depth of the well at >5000 m. Although 21 jars were fired for stacking purposes, they were not sufficiently energetic to be detected at all stations. Only S-waves were detected at Otterbach 2 and Haltingen.

The second option was a combined determination of hypocenter locations and velocities. To minimize nonuniqueness in the solution, a deep geophone in the reservoir interval was required. The only option was to deploy a tool into the stimulation well, Basel 1. However, the tool could only be deployed at the start of the stimulation.

Over the 40 hours of deployment, event locations were predominantly within 100 m of the geophone. Two types of response were observed. In the first, a single arrival was detected as illustrated by one of the earliest microseismic events to be located, around seven hours after the start of the stimulation (Figure 3a). The second response pattern, illustrated by an event 30 hours after the start of the stimulation (Figure 3b), has two arrivals, interpreted to be the P- and S-waves. The minimum traveltime separation of the P and S arrivals

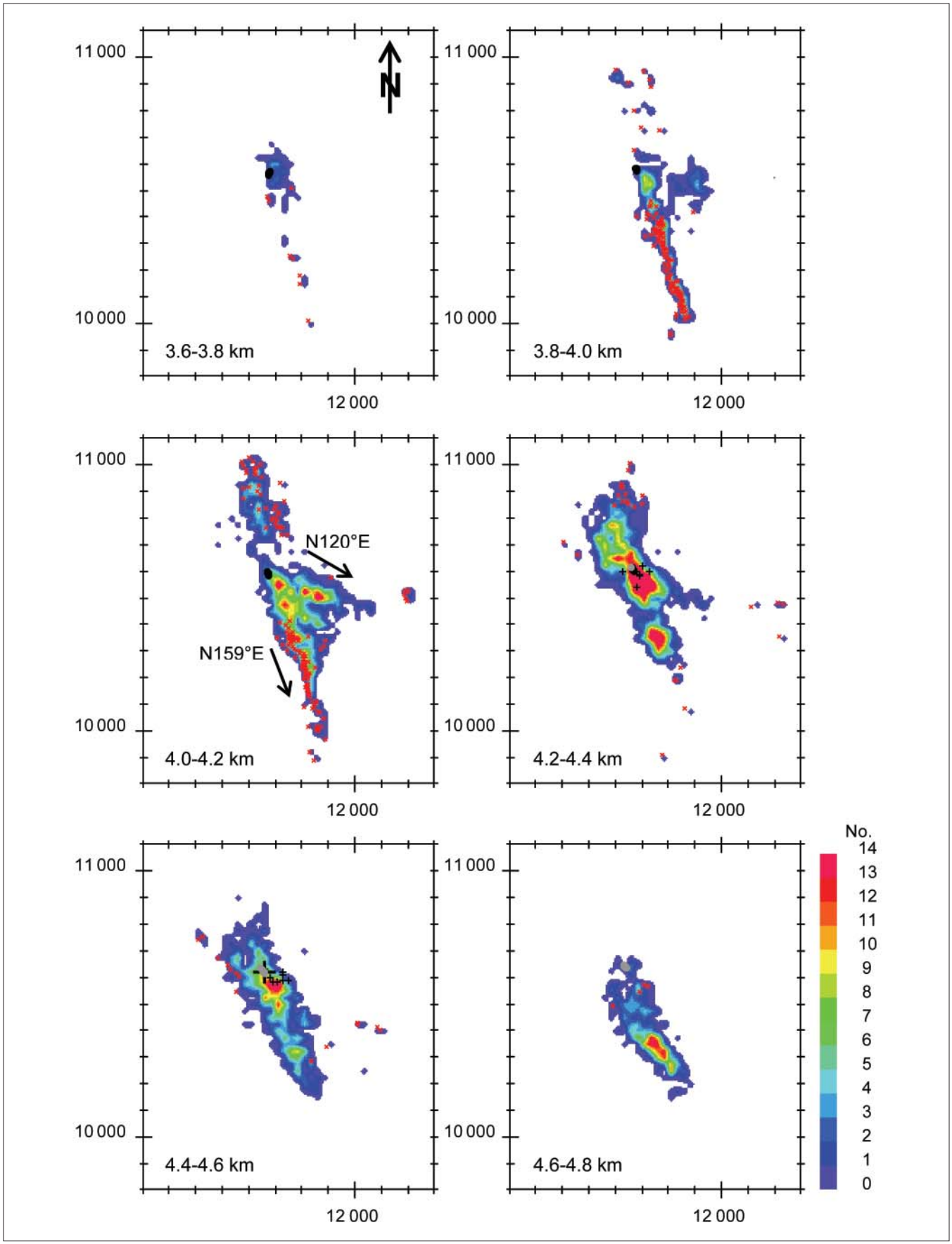

Figure 6. *Depth slices between 3.6 and 4.8 km bOD showing contours of the number of seismic events during the main and poststimulation phases in a grid of cells 25 × 25 × 200 m. The depth range bOD of each slice is annotated in the bottom left corner. The pre- and poststimulation events are overlain as black and red crosses, respectively. The projection of the Basel 1 borehole in each depth section is shown in black for the cased section and grey for the openhole. The large black cross in the 4.4–4.6 km section indicates the location of the Basel 1 geophone.*

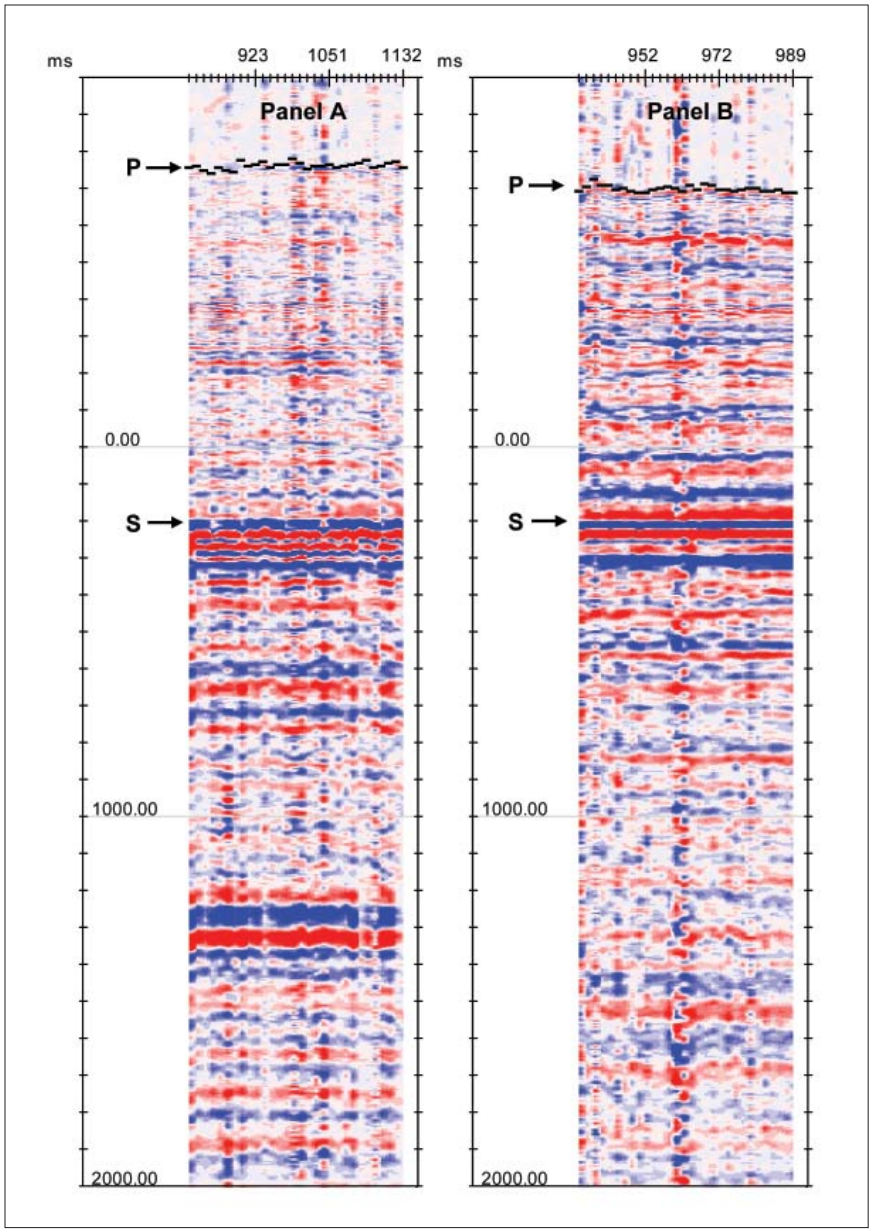

Figure 7. *Common-receiver gathers of the vertical trace at Schützenmatte. Panel A covers a 12-hour period at the start of the stimulation. Panel B covers an 8-day period three months after the stimulation. The traces have been aligned with the direct S-wave at 200 ms. The P-wave picks are indicated by horizontal black bars. DC removed, trace-by-trace scaling, 300% overlap.*

that could be resolved corresponded to hypocenter distances of around 50 m. Thus, events for which the P and S arrivals could not be distinguished were even closer to the geophone.

The early events where the P and S arrivals were indistinguishable could be treated essentially as check shots with the shot instant being detected by the deep geophone. The onset of the event in Figure 3a was taken as time zero of the event and the model granite P- and S-velocities were simply set at the average velocities from the deep geophone to Otterbach 2. The P- and S-velocities in the sediments were found by iteratively ray tracing from the deep geophone to the network to find the velocities with the minimum rms traveltime misfit.

The two-layer model provided reasonable traveltime fits, with residual errors of up to 23 ms to all the stations except Riehen 2 where the residual P and S misfits were 73 and 97 ms, respectively. The Riehen 2 misfits indicate that the velocities are lower to Riehen 2 than to the other receivers. This may be related to faults within a flexure zone near Riehen 2 (Figure 1). However, as the seismicity originates from a relatively small region, the raypath differences to the sensors due to different event locations will be correspondingly small. As a result, for location purposes, the residual misfits may be removed by static corrections for each receiver station.

Microseismic data processing and hypocenter location

The acquisition system produced a continuous stream of trace files containing 30 s of data. Successive files were read by the processing software to search for prospective microseismic events. In general, a potential event could be reliably identified if the amplitude level at Otterbach 2 exceeded a specified background level as this sensor had very low environmental noise relative to the rest of the network.

If a potential event was detected, the trace data from all sensors were extracted for a time window (1 s before until 4 s after the trigger). An automatic process attempted to pick the P and S times of each new event and perform a location. This was supported by visual interpretation and typically required two interpreters to keep up to date during the stimulation. Around 90% of the total event locations were processed in near-real time with this method. The remaining events were located subsequently using visual checks to identify missed events and to ensure consistency in the traveltime interpretation.

The location process was an exhaustive grid search in which an initial coarse location was found using a 25-m cubic grid. A 2-m cubic grid was used to refine the location. For every location, P and S times from Haltingen, Schützenmatte, Riehen 2 and Otterbach 2 were required. (The P times from the deep geophone in Basel 1 were also used when this receiver was deployed.) For consistency in locations, any other times were excluded. The hypocenter locations have a maximum rms misfit of 10 ms. Events with larger misfits were not located.

Moment magnitudes were derived from the principal component of the triaxial sensors required in the location using the spectral method of Abercrombie (1995).

Microseismic monitoring and event distribution

Prior to the main stimulation, 16 locatable microseismic

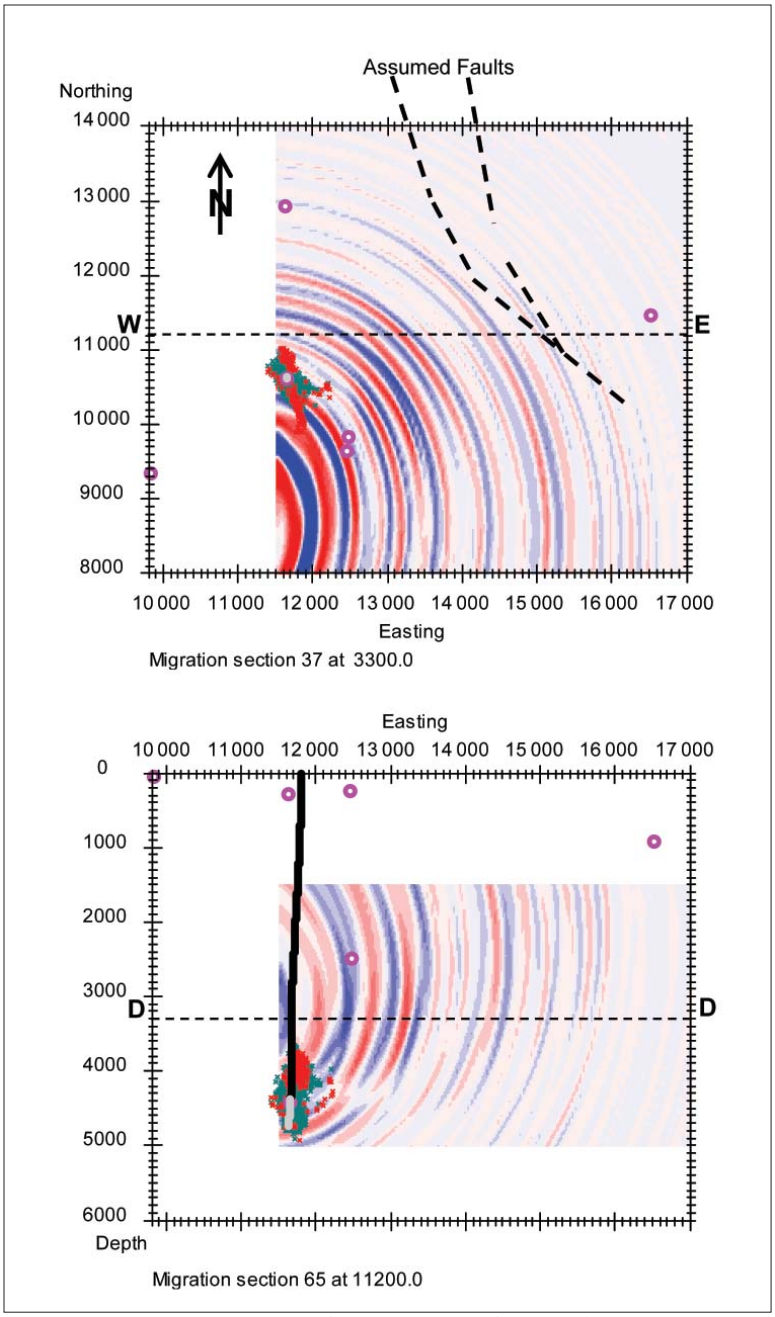

Figure 8. *S-wave migration at Schützenmatte in a horizontal section (top) at a depth of 3300 m and a vertical WE section (bottom) at 11 200 m north. The intersection of the vertical section with the horizontal section is indicated by the WE dotted line and the intersection of the horizontal section with the vertical section is indicated by the dotted line DD. The assumed faults previously shown in Figure 1 are overlain in the horizontal section for reference and the horizontal section is outlined in green on the map in Figure 1. The main stimulation and poststimulation events are shown as green and red crosses, respectively. The cased section of Basel 1 is shown in black and the openhole is grey. Pink circles mark the microseismic monitoring network stations. Schützenmatte is west of the figure boundaries.*

events were detected. The first four coincided with an inflow of water during a drilling operation after the well had reached 4688 m bOD and a further eight events were located while the well was being cemented. Subsequently, an injection test was performed in which the pressure was increased very slowly in order to identify the stimulation pressure for seismicity. Initially, events occurred sporadically every hour or so. When the surface pressure reached 5 MPa, the event rate increased to 14 per hour and subsequently continued to increase in line with the rising pressure. However, only four events detected during this prestimulation test were locatable. All events prior to the main stimulation occurred close to a permeable zone at 4422 m bOD.

Figure 4 shows the injection rate and wellhead pressure during the main stimulation and the located microseismic event rate. On 8 December 2006, an event of 2.6 M_L occurred at 03:06 that had a PGV of 0.55 mm/s. As a precaution, the injection rate was reduced to 1800 l/minute at 04:04 and, following further events of >2.0 M_L, the injection was stopped at 11:34 and the well shut in. However, a 2.7 M_L event occurred at 15:46 followed by a 3.4 M_L event at 16:48 on the same day and so, in accordance with the response strategy the well was bled off.

A total of 13 500 potential events were detected; 3124 were located in the period 2–12 December 2006, covering the main stimulation and decline in the event rate. During the poststimulation period, a further 350 locatable events were detected up to 2 May 2007 by which time events were occurring sporadically (about one per day). All seismicity located during the main stimulation is shown in a 3D view in Figure 5; the events have been scaled according to their moment magnitudes. More than 80% of the events have misfits of less than 8 ms, the picking error used to estimate the resolution, which suggests that the resolution estimate of 100 m is reasonable. The total volume of the active region has been estimated by summing the volume of a grid of 25-m cubic cells that contain at least one event. This produced a volume of just over 35 $\times$ 10^6 m^3.

Figure 6 shows the event locations during the main and poststimulation for a series of depth slices at 200-m intervals. Each slice is a contour plot of the number of events in a grid of cells of 25 $\times$ 25 m in the horizontal plane and 200 m in depth.

The depth slices show that the events fall on relatively narrow features. Two distinct orientations can be seen in the microseismicity at N159°E and N120°E (depth section 4.2–4.4 km). The poststimulation events south of Basel 1, in particular, lie close to a single plane in the dominant orientation, N159°E. This alignment is similar to the directions of SHmax estimated from borehole breakouts at N143±14°E and from drilling-induced tensile fractures at N151±13°N and also with the majority of natural fracture orientations in the granite that were in the azimuth range N140°–170°E. In comparison, there were relatively few natural fractures around N120°E which may explain why the microseismic alignments are significantly less developed in that direction. Since the expected resolution is around 100 m, the features in the depth slices could be interpreted as a single fracture surface in the dominant direction with some smaller branches.

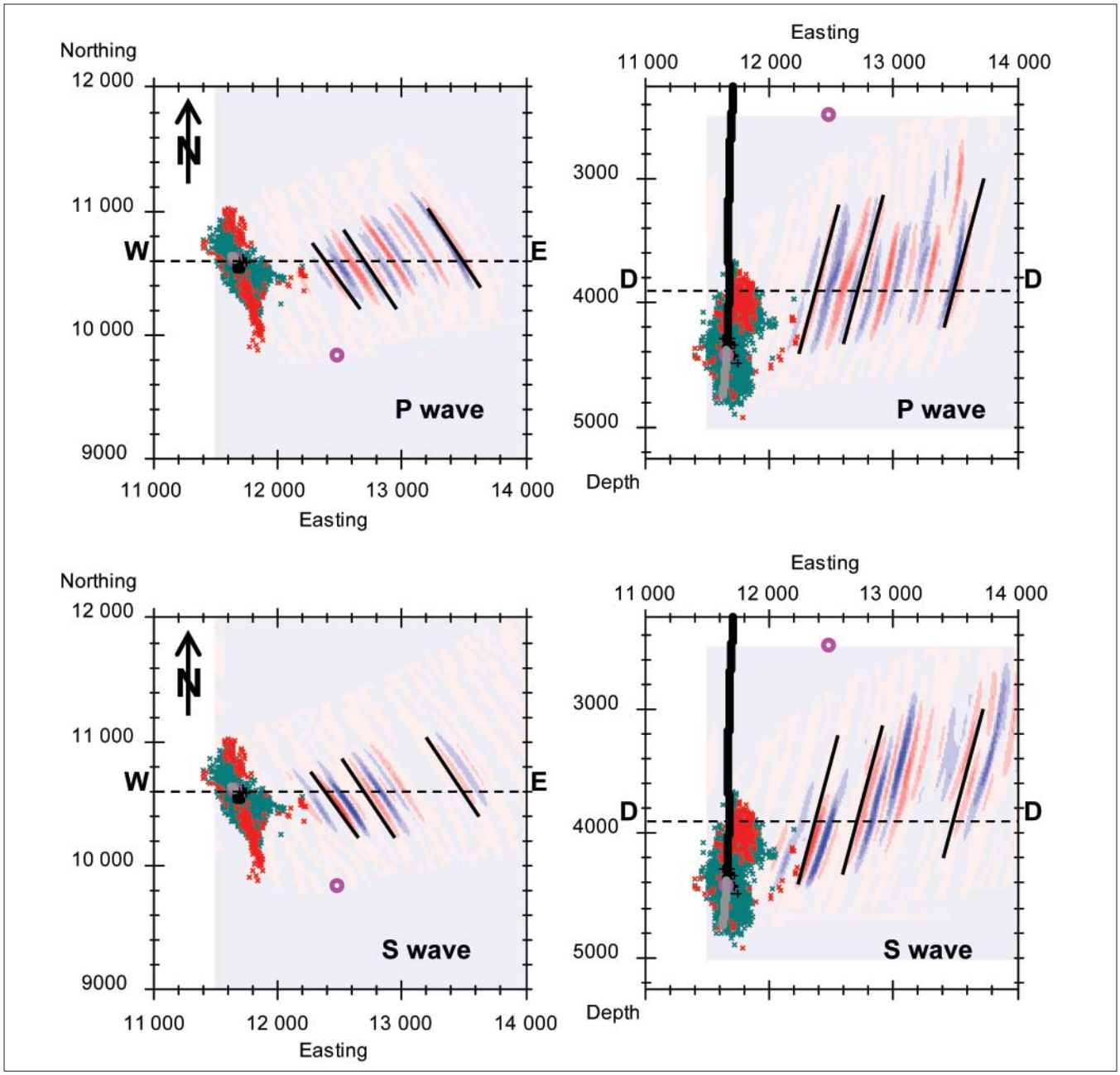

Figure 9. *The P-wave and S-wave migrations with aperture control at Schützenmatte in horizontal sections at 3900 m (left) and vertical WE sections at 10 600 m north (right). The intersections of the vertical sections with the horizontal sections are indicated by the WE dotted lines and the intersections of the horizontal sections with the vertical sections are indicated by the DD dotted lines. The black lines indicate the strike and dip of the three interpreted reflections. The prestimulation, main stimulation and poststimulation events are shown as black, green, and red crosses, respectively. A 500-m, low-pass filter has been applied from left-to-right across the sections. The cased section of Basel 1 is black and the openhole is grey. The pink circle is the Otterbach 2 station.*

Migration

Potential reflections within the microseismic data are of interest because they offer the possibility of imaging fractures not seismically active during the stimulation. Such fractures might be targeted by subsequent stimulations or drilling to expand the reservoir. Place et al. (2006) illustrated how steeply dipping faults offset from a geothermal well may be imaged using VSP. Here it is shown how potential fractures several kilometers from the stimulation well may be imaged by migrating the microseismic trace data.

When the trace data for the located events are displayed for an individual sensor and aligned at either the P or S first arrival picks, near-parallel secondary arrivals can be seen (Figure 7). These arrivals are most consistent when the event locations are closest, such as early in the stimulation (panel A) and so were thought to be potential P and S reflections. In an eight-day period around three months after the stimulation, a group of events within ~200 m of each other occurred on the southern edge of the reservoir. The traces from these events (panel B) also have consistent secondary arrivals but at different times to those in panel A due to source locations ~800 m away.

In order to image the potential reflectors, a 3D diffraction stack-type migration (e.g., Chavarria et al., 2003) was applied

to the events located during the stimulation and poststimulation up to 2 May 2007. P-wave images were formed separately by applying a tapered mute prior to the direct S-wave arrival. The signal-to-noise ratio of the P-wave was strongest on the vertical traces as would be expected, and so the P-wave migration images were formed using the vertical traces only. The S-wave arrival was strongest on one of the horizontal traces. The horizontal trace with the best signal-to-noise ratio was used to form the S-wave migration images. In this case, a mute was applied to eliminate the direct P- and S-waves.

Each sensor was migrated separately as the sensors were too widely spaced to produce continuity in a stacked image of more than one sensor. Initially no constraints were applied to the dip and azimuth of the reflectors in the images. For example, horizontal and vertical sections through the Schützenmatte S-wave migration are shown in Figure 8. Two assumed faults from Figure 1 have been overlaid. While it is interesting to note the coincidence of migration features and the fault traces in the horizontal section, the migration data are not sufficiently reliable to be correlated with the assumed faults to make an interpretation.

Steeply dipping features aligned around N150°E appeared to be preferentially enhanced in all images northeast of Basel 1. The images west of Basel 1 showed no preferential directions of stack response and are not considered here. In order to optimize the observed alignments, secondary migration of the region east of Basel 1 was performed with an aperture control applied to constrain the azimuth of the reflectors to N150±5°E. The dip was constrained to 87±5° in the direction N240°E in keeping with the overall dip of the microseismicity. Beyond this range the trace amplitudes included in the stack were tapered linearly to zero over a further 5°.

Figure 9 shows sections through the Schützenmatte P- and S-wave migration with aperture controls for sections with the maximum amplitude. The P-wave images cover a smaller region than the S-wave images due to the limited trace range between the direct P- and S-wave arrivals that could be migrated as potential P wave reflections. The P-wave image has lower resolution due to longer wavelengths.

There is reasonable consistency between the P- and S-wave images in Figure 9. All suggest the possibility of three reflectors east of the event locations (indicated by black lines overlying the P- and S-wave images). The strike of these features is around 145° and consistent with the overall strike direction of the microseismicity. The apparent dips are less than the overall dip of the microseismicity and are around or less than the shallow dip extent of the allowed dip range. This may be caused by migration smearing rather than the real dip.

The features are offset 600, 1050, and 1600 m from Basel 1 and so of interest for targeting further boreholes. However, these potential reflectors are not imaged unambiguously. The limited distribution of events and migration of a single sensor means that the migration process cannot stack out noise effectively, and there is a possibility that the images are migrated noise. To obtain more reliable images, more receivers would be required either by expanding the network considerably or

by deploying a multilevel string in one or more boreholes.

Discussion

The estimated and stimulated volume containing seismically active fractures is of the order of 10% of the target volume of 400×10^6 m^3. Because of the occurrence of larger seismic events, it is not yet clear whether further work to enhance the fractured volume can be performed. While the intention was to produce microseismicity associated with fracture opening to improve the injectivity of the reservoir, the events were larger than anticipated based on previous experience at other HDR sites. This problem is the subject of continuing research.

Nonetheless, the subject of this paper, the microseismic monitoring system, was reliable and a technical success. In cooperation with the SED, earthquake magnitudes were derived in near real time and published on the Web for public information. Although the larger earthquakes were undesirable, the response strategy provided an effective means of dealing with these events in a consistent manner and was essential in fulfilling the company's overriding commitment to public safety. The microseismic system also provided important technical information for monitoring and evaluating the hydraulic stimulation as the event locations and time history enabled the growth of the stimulated region and its dimensions to be assessed in near real time.

It appears that the stimulation has produced a relatively thin fractured region or possibly a single fracture surface with a few smaller branches providing additional lateral extent. The overall reservoir strike direction is consistent with the azimuth of SHmax and the strike direction of natural fractures within the crystalline section from log analysis. Imaging the fine structure of the reservoir has been possible because of the relatively good resolution of the event locations. This was due to a combination of careful traveltime interpretation, consistent location criteria and a reliable velocity model.

Obtaining the velocity model from geothermal wells can be difficult using check shots due to the high temperatures and pressure conditions downhole. One alternative method using drilling jars had only limited success. A second, novel method (using a high temperature and pressure geophone tool in the injection well) succeeded, was relatively economic, and involved much less risk to the well.

It has also been shown how 3D migration can image potential fracture zones that have not been stimulated. This technique could be significant in planning the trajectories of subsequent wells.

Suggested reading. "Earthquake source scaling relationships from –1 to 5 M_L using seismograms recorded at 2.5 km depth" by Abercrombie (*Journal of Geophysical Research,* 1995). "Creation of an HDR reservoir at 5000 m depth at the European HDR project" by Baria et al. (Proceedings of the 31st Workshop on Geothermal Reservoir Engineering, Stanford University, 2006). "Microseismic monitoring of the world's largest potential HDR reservoir" by Baria et al. (Proceedings of the 29th Workshop on Geothermal Reservoir Engineering, Stanford University, California, 2004). "A look inside the San Andreas fault at Parkfield through vertical seismic profiling" by Chavarria et al. (*Science,* 2003). "The state of stress in northern Switzerland inferred from earthquake seismological data and in-situ stress measurements" by Evans and Roth (final report, Deep Heat Mining, DHM, Steinmaur, Switzerland, 1998). "Control of hazard due to seismicity induced by a hot fractured rock geothermal project" by Bommer et al. (*Engineering Geology*, 2006). "Oriented three components VSP method applied to imaging highly dipping faults in the deep granite basement at Soultz-sous-Fôrets" by Place et al. (ENGINE workshop, Potsdam, 2006). "The stress field in the Rhine Graben area inferred from earthquake focal mechanisms and estimation of frictional parameters" by Plenefisch and Bonjer (*Tectonophysics,* 1997). "Stress orientation at the Basel geothermal site from wellbore failure analysis in Basel 1" by Valley and Evans (ETH Report 3465/56, 2006). TLE

Acknowledgments: We thank the investor group Geopower Basel AG for financial commitment and support. The authors gratefully acknowledge the continuing contribution of the Swiss Seismological Service. Expert advice in ground velocity measurements was provided by Adrian Egger of Rutishauser Ingenieurbüro GmbH. The hydraulic data were diligently acquired by GEO-data, and we are indebted to Claudio Forlin for prompt IT support. The acquisition system was supplied by Reftek. Network sensors were supplied by Sondi and Consultants. The processing software and high temperature and pressure seismic tools used in Basel 1 were supplied by Semore Seismic.

Corresponding author: bdyer@seismics.net